Study on the aggregation of DNA capped gold nanoparticles: a smart and flexible aptasensor for spermine sensing

Tik-Hung Tsoi[a], Yan-Juan Gu[a], Wai-Sum Lo[a], Wai-Ting Wong[a], Wing-Tak Wong*[a], Chi-Fai Ng*[b], Chi-Sing Lee*[c], Ka-Leung Wong*[d]

[a] T.H. Tsoi, Dr. Y.J. Gu, Dr. W.S. Lo, Dr. W.T. Wong, Prof. W.T. Wong, Department of Applied Biology and Chemical Technology, The Hong Kong Polytechnic University, Hung Hom, Hong Kong SAR.
E-mail: w.t.wong@polyu.edu.hk

[b] Prof. C.F. Ng
SH Ho Urology Centre, Division of Urology, Department of Surgery, The Chinese University of Hong Kong, Shatin, N.T., Hong Kong SAR
Email: ngcf@surgery.cuhk.edu.hk

[c] Dr. C.S. Lee
Key Laboratory of Chemical Genomics, School of Chemical Biology and Biotechnology, Peking University Shenzhen Graduate School, China
Email: lizc@pkusz.edu.cn

[d] Dr. K. L. Wong
Department of Chemistry, Hong Kong Baptist University, Kowloon Tong, Hong Kong SAR.
Email: klwong@hkbu.edu.hk

Supporting information for this article is given via a link at the end of the document.

Abstract: Current screening methods towards prostate cancer are not without limitations and lead to a controversial screening outcome. Recently we have discovered the usefulness of urinary spermine as a secondary screening test to supplement the commonly adopting serum Prostate Specific Antigen test. In this study, we developed a smart gold nanoparticles based aptasensor for the sensing of this biomarker in a convenient and fast manner. A comprehensive study was performed to elucidate the driving force of DNA adsorption, different factors' effect, like gold nanoparticles size, DNA length, concentration and working pH towards spermine sensing by using UV-Vis Absorption Spectroscopy and Isothermal Titration Calorimetry. It was found that the developed aptasensor could smartly detect spermine via two different sensing mechanisms simply by adjusting the DNA concentration without complicated procedures. Good performance in complicated matrices was proven by the satisfactory results obtained in the spike analysis of both artificial urine and clinical urine samples. Such a flexible and smart approach described here would provide a useful tool for the fast sensing of spermine and prostate cancer screening.

Introduction

The polycationic polyamines putrescine, spermidine and spermine (SPM) are essential regulators of several cellular processes including cell growth and proliferation.[1-4] Research on this group of analytes could date back several centuries and had proven their effects through regulating specific gene expression and ion channels, associating with different nucleic acids and maintaining chromatin conformation, membrane stability and free-radical scavenging.[5-10] Owing to their active participation into numerous metabolic pathways, their contents, especially urinary contents, were considered to be potential biomarkers for monitoring different types of growing tumours and following medical treatment for cancerous patients. One of the most promising finding reported by Russell's group in the late 1960s was a considerable increase of ornithine decarboxylase, a key enzyme for polyamine production, as well as urinary polyamines
contents in patients with various types of solid tumors and leukaemias.[11-12] Afterwards, specific polyamine studies focusing on different types of cancers continued to further elucidate the their potential role as a prognostic marker.[13-15]

Our group concerns the current medical challenge on screening of prostate cancer (PCa). Currently adopting methods like Digital Rectal Examination, Prostate Specific Antigen (PSA) test and transrectal ultrasound guided prostatic biopsy all have their own limitations and are not perfect to be used as a screening method.[16-20] To address this issue, previously we had reported results of our biomarker validation study in a large PCa patient cohort on urinary polyamines.[21] Usefulness of urinary SPM was demonstrated to successfully differentiate patients either having PCa or Benign Prostatic Hyperplasia, which allows it to act as a secondary screening tool to assist serum PSA test and address its high false-positive rate when using 4.0ng/ml as a cut-off point.

To assay polyamine contents, classical analytical techniques such as chromatographic techniques coupled with different detectors, capillary electrophoresis or immunoassays are still primarily used nowadays.[22] Most of these techniques are expensive, time-consuming and require experienced technical staffs to handle their operation and tedious sample-pretreatment or derivatization steps. Development of fast kits towards these chromophore-free analytes is therefore a hot area of research in analytical fields.[22-24]

Gold nanoparticles (AuNPs) emerged as a biocompatible nanomaterial and have been widely used in biomedical engineering and bioanalytical applications.[25] For example colorimetric biosensing probes towards a wide variety of chemical species were developed based on the red-shifting of their unique Surface Plasmon Resonance band.[26-28] Response can be viewed directly by naked eye upon any modulations of the aggregation state by the target analyte. Several reports had previously demonstrated the use of AuNPs for polyamine sensing via different approaches, especially the approach of using bare AuNPs which could achieve a sensitive SPM detection in urine down to 10ppb.[29-31] Another interesting article was reported by Liu et al. about the use of ssDNA-capped AuNPs to achieve SPM sensing based on a non-crosslinking mechanism, while leaving a lot of unanswered questions.[32] Therefore in this report we performed a more comprehensive study on this phenomenon. Different factors' effects, including the AuNPs size, DNA length, concentration, working pH towards SPM sensing were carefully elucidated and provided us more hints about the role of DNA aptamer as well as the two sensing mechanisms of aptasensor: depending on the amount of DNA being added, it either sensed SPM based on the aggregation of DNA-AuNPS which resulted in the red-shift of plasmonic band, or the precipitation of DNA-AuNPS which resulted in the decline of plasmonic band. (Figure 1) This design has a potential to be a useful kit for a fast sensing of SPM and therefore screen out prostate cancerous cases, improving the outcome of PCa screening.

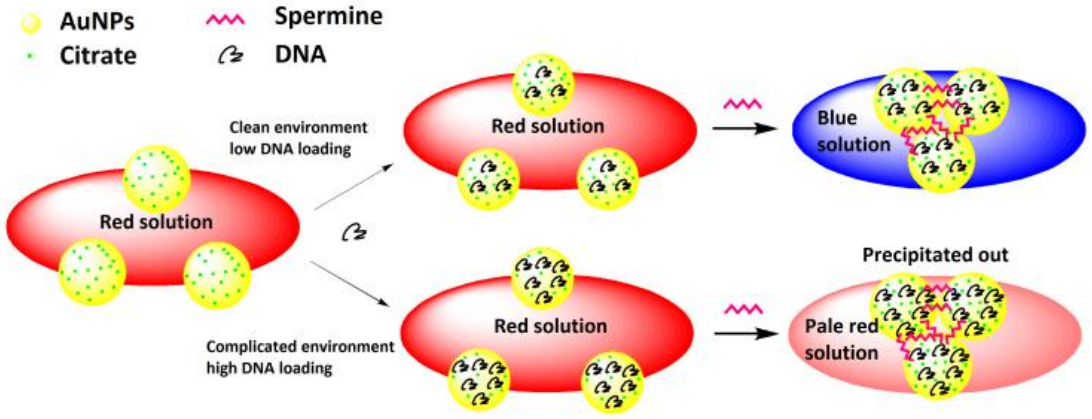

Figure 1. Schematic diagram of the developed aptasensor for SPM sensing via two different pathways. Different amount of DNA was adsorbed onto AuNPs by displacing the original citrate surfactants. Later addition of positively charged SPM would induce either the aggregation of DNA-AuNPs which resulted in a red shift of plasmonic peak, or the precipitation of DNA-AuNPs which resulted in a decline of plasmonic band absorbance.

Results and Discussion

Study on effects of different factors

Sensitive and specific sensing towards SPM was achieved by our developed aptasensor via two stages according to Zhang's binding model.[33] The first stage, as being demonstrated in Figure 1, started with the selective adsorption of DNA aptamer onto the surface of citrate-AuNPs. Citrate ligands were being displaced since DNA could adopt an extended conformation to strengthen its binding with AuNPs surface. This could be viewed from our DLS result that with more DNA, the hydrodynamic size of AuNPs became smaller and smaller due to the displacement of citrate layer by a more compact DNA molecule for protecting AuNPs against acidic condition. (Figure S1) This protection effect was also shown in another experiment (Figure S2), which clearly demonstrated that the aggregation driven by the presence of salt had slowed down at a high DNA capping condition. The second stage was the addition of positively charged SPM for inducing further DNA adsorption by shielding the negative charges on both AuNPs and DNA aptamer, and as results weakening the repulsion force for AuNPs aggregation. The extent of aggregation would therefore allow an indirect quantitation of SPM content

in a convenient and fast manner.

To further study the driving force of citrate displacement by DNA, it was well studied before and proposed to be caused by the presence of positively charged sodium salt (e.g. NaCl) that would screen the charge repulsion between the negatively charged AuNPs and DNA.[33] In our case, the AuNPs were used directly after synthesis without any clean-up. Therefore a lot of free sodium citrate/sodium borohydride and side products would act as such screening sources for DNA adsorption. A proof-of-concept experiment was performed to remove these free inorganic salts by ultrafiltration using a filter with a pore size large enough for them to pass through. (MWCO = 30kDa) The removal was confirmed by checking the sodium content by ICP-OES. (Figure S3) After ultrafiltration, the AuNPs was reconstituted with water and they didn't show significant aggregation as confirmed by both UV-Vis absorption measurement and TEM analysis. (Figure S4 and S5) When DNA was mixed with these ultrafiltration-treated AuNPs in acidic BR buffer, solution turned dark purple immediately indicating aggregation. Vice versa, the solution color remained red in case of untreated AuNPs. This proved that the presence of free inorganic salts from starting materials were important for DNA to adsorb and exert its protection effect to AuNPs. Working condition parameters as discussed below were studied and optimized carefully so as to maximize the analytical performance of the aptasensor for SPM sensing in urine. This was achieved by studying the slope of SPM calibration graphs, which reflects the corresponding sensitivity in each case, and the linear working range to fit the usual urinary content of SPM. The first parameter we studied was the size effect of AuNPs. Different sizes of AuNPs (4, 13 and 27nm) were all prepared using sodium citrate as surfactant. (Figure 2) As being illustrated in Figure S6, by taking logarithm on the absorbance ratio at 610nm and their plasmonic peaks, the sensitivity becomes greater and linear range become narrower with the increase of AuNPs size. Considering the fact that most urine samples are having urinary SPM content in the range of 0-15μM, 4nm AuNPs seemed to be the best choice for later experiments by providing the widest and most appropriate linear working range. And to explain such an observation of trend, it was believed that the number of AuNPs was smaller in cases of larger AuNPs, thereby more easily getting aggregated as induced by the same amount of SPM being added into the AuNPs solution.

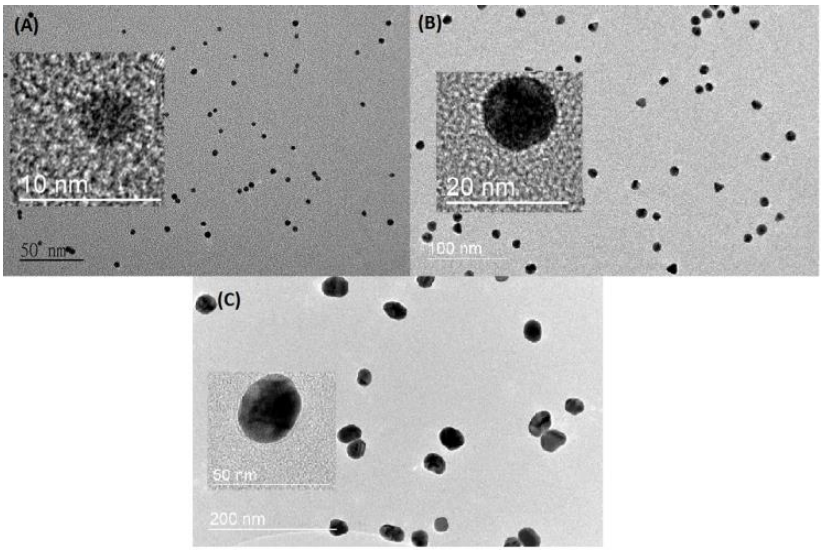

Figure 2. TEM images of citrate-AuNPs. (A) 4nm (B) 13nm (C) 27nm. Inset: Magnified TEM image.

The second parameter was the DNA concentration. Basically in all cases the curve showed a linear range initially, which then gradually leveled off. (Figure S7 and Table S1) And with more DNA, a wider linear working range was obtained with a compensation of sensitivity. Due to the nature of single strand DNA easily being adsorbed onto AuNPs, in this method it omitted the need to prepare DNA-AuNPs through tedious target-directed surface modifications. Flexibility was therefore conferred on users to tune the working range simply by changing the DNA amount added to AuNPs. Finally, 25nM was chosen as the optimal concentration to provide the best sensitivity.

The third parameter was the pH. (Figure S8 and Table S2) Our results showed that the aptasensor worked better in acidic medium, which was essential to maintain SPM in its +4 charge state. (pKa = 7.90, 8.83, 9.97 and 10.79) A low pH condition also helped DNA to adsorb onto AuNPs more easily.[37] Finally 3.29 was chosen as the optimal pH.

For the effect of DNA length, a longer aptamer is known to adsorb with a higher stability for protecting AuNPs better from aggregation.[33] (Figure S9) When considering the absorbance change upon addition of same concentration of SPM solution, 24-mer was the greatest so it was chosen. The last parameter was the incubation time by monitoring the aggregation kinetics, and it was determined that 60 min was sufficient for reaching an equilibrium state. (Figure S10)

Under the optimal conditions in a blank matrix, by taking logarithm on the absorbance ratio, a linear SPM calibration curve from 0-5μM could be fitted by the least square linear regression. (Figure 3) The equation was y = 0.1029x - 0.4941, with limit of detection (LOD) calculated to be 15.25nM (3.09ng/ml) by the equation of LOD = 3σ of absorbance in the absence of SPM / slope of curve.[34] TEM images clearly showed the increase of AuNPs aggregation extent in an increasing amount of SPM content. (Figure 4) DLS and zeta-potential were also measured under the described conditions. (Figure S11) The hydrodynamic size increased with an elevating SPM concentration for causing a larger degree of aggregation, but unlike the results from Liu et al. for 13nm AuNPs, our results showed that the zeta-potential of 4nm AuNPs remained nearly constant instead of gradually restoring to a more positive level.[32] This might be due to most SPM molecules being embedded in the core of aggregates.

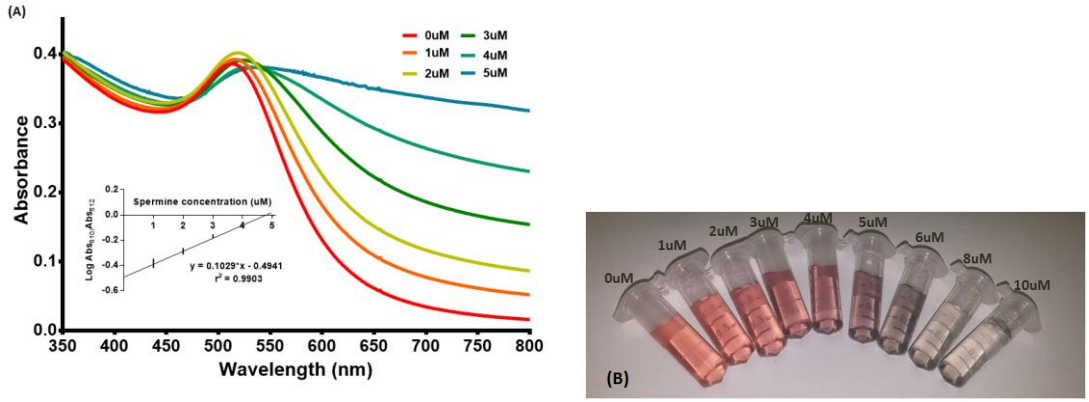

Figure 3. The SPM induced aggregation on DNA-AuNPs in blank matrix - The absorption spectra of DNA-AuNPs upon addition of SPM solution. (0-5μM) Inset: Plot of normalized Abs_{610}/Abs_{512} vs SPM concentration. (B) The photo of AuNPs solution color with different extent of SPM induced aggregation. (0-10μM)

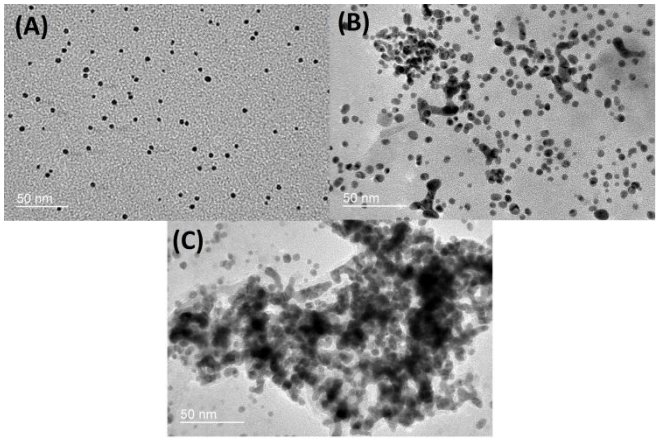

Figure 4. TEM images of DNA-AuNPs (A) in the absence of SPM (B) in the presence of 2μM of SPM (C) in the presence of 5μM of SPM. (Concentration: AuNPs = 80nM; DNA = 25nM; BR buffer = 4mM, pH 3.29)

Mechanistic study on AuNPs aggregation

During the study of DNA concentration effect, it was interesting to observe a drop of sensitivity towards SPM when more DNA was added during the assay. This contradicted to the previous suggestion that SPM-induced aggregation occurred through DNA molecules via an ion-bridging effect and non-crosslinking mechanism.[32] A control experiment in the absence of DNA was therefore performed to gain more information. It was found that the SPM-induced aggregation process could still be observed and even exhibited with the fastest aggregation rate when compared to conditions with the presence of DNA. (Figure S12) It seemed the presence of citrate groups originally capped on AuNPs could not be neglected and they contributed significantly to the aggregation process.

To have a deeper insight into the mechanism, we performed several Isothermal Titration Calorimetry (ITC) experiments: Same amount of citrate capped AuNPs was firstly mixed with different concentration of DNA (0, 0.5, 1 and 3μM) separately. SPM solution was then added gradually for measuring the temperature change in each injection. The data in each case were being shown respectively in Figure 5 and the overall results were summarized in Table 1 below.

In each case the binding isotherm showed an enthalpic peak deviating from the fitting model. Rautaray et al. reported a similar observation when they studied the interaction of Ca^{2+} ions and aspartic acid-capped AuNPs, suggesting the peak was due to the aggregation of AuNPs as a consequence of neutralization of charge by Ca^{2+} ion.[35] This statement seemed reasonable when being applied in our case. When more DNAs were being added, we could observe the enthalpic peak gradually shifting to a higher molar ratio of SPM to AuNP, implying that the AuNPs aggregation could only be initiated at a higher concentration of SPM. This matched well with the results from UV-Vis absorption measurements which revealed the drop of sensitivity towards SPM at a higher DNA concentration. Analyzing the thermodynamic parameters carefully, we knew that SPM-induced aggregation of AuNPs mainly happened via an enthalpy-driven electrostatic/hydrogen-bonding interaction

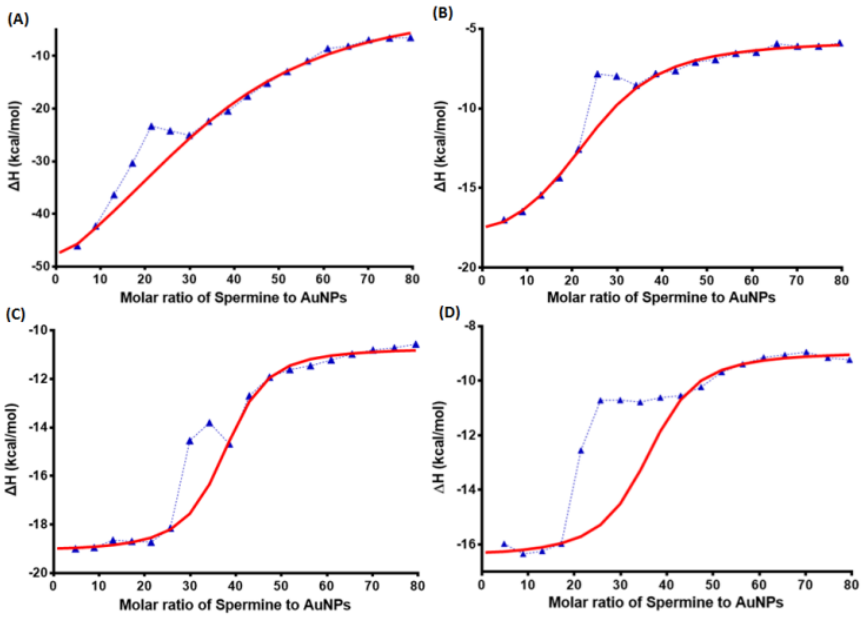

Figure 5. Integrated ITC titration curve at different DNA concentration. (A) 0μM (B) 0.5μM (C) 1μM (D) 3μM. Red curves indicate the fitting line of data points using the single binding site fitting model.

Table 1. Thermodynamic parameters of the binding of SPM to AuNPs at different DNA concentration. (0-3μM) (K_D: dissociation constant; ΔH: enthalpy change; ΔG: Gibbs free energy change; T: temperature in Kelvin (298K); ΔS: entropy change)

DNA concentration (μM)	K_D (μM)	ΔH (kcal/mol)	ΔG (kcal/mol)	TΔS (kcal/mol)
0	8.13	-67.9	-6.95	-61.0
0.5	2.03	-13.4	-7.77	-5.68
1	0.345	-8.40	-8.82	0.418
3	0.472	-7.52	-8.63	1.12

as reflected from the larger and negative values of ΔH. The entropy component gradually became more favorable as the DNA concentration increased, but it was still weaker and enthalpy remained as the major driving force. Similarly Morgan et al. reported long time ago that SPM interacts with DNA primarily through electrostatic interaction, while minor non-electrostatic interactions are also present.[36] It was similar to the results of our later ITC experiment on DNA and different polyamine analogs. (Table S4) Therefore, the gradual drop of ΔH strength with increasing DNA concentration implied the weakening of such electrostatic/hydrogen-bonding interactions. From these results, we hypothesized SPM interacting with AuNPs electrostatically primarily through the surface citrate ligands, but not the DNA aptamers. The role of DNA in the current developed aptasensor was to displace surficial citrate ligands for providing a better protection to AuNPs, and concurrently to control the extent of the major citrate-SPM interaction, AuNPs' aggregation rate and therefore the analytical performance of the aptasensor.

To confirm the importance of surficial citrate during aggregation, we performed another ITC experiment for

studying the interactions between pure citrate ligands and other polyamine analogues. While there are three carboxylate groups in a free citrate ligand for interacting with SPM, the conformation is different when being capped onto AuNPs. On average there may be only one free carboxylate group available on each citrate ligand for interaction, according to the proposed configurations by Park et al.[37] Despite this structural difference, the cross-reactivity sequence determined from UV-Vis absorption measurements of AuNPs (SPM > Spermidine > Histamine > Putrescine = Arginine = Tyramine = Cadaverine = Ornithine = Control) was similar to that of the ΔH strength sequence obtained from the ITC profile of free citrate (SPM > Spermidine > Histamine > Putrescine > Arginine > Tyramine = Cadaverine = Ornithine = Control), but not to that of the DNA. (Table S3 and S4 for the summarized thermodynamics data of free citrate and DNA obtained from ITC; Figure 6 for the selectivity data obtained from UV-Vis spectroscopy) This result might indirectly imply the importance of surficial citrate in achieving aggregation.

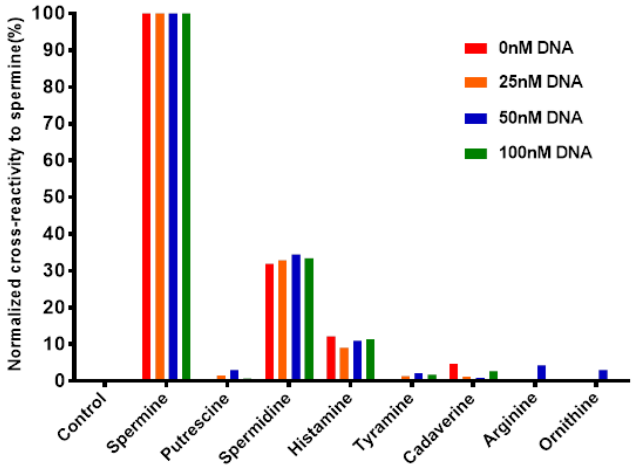

Figure 6. Selectivity profile of aptasensor against polyamine analogs at different DNA concentration (0, 25, 50 and 100nM). In each case control (water) and SPM were normalized to 0 and 100% respectively. (Polyamines concentration used = 5μM)

To further show that DNA only played a minor role in the interaction with SPM in causing aggregation, the selectivity profile of AuNPs against polyamine analogs at different DNA concentrations was monitored. Each of their cross-reactivity was determined by comparing the Abs_{610}/Abs_{512} to that of SPM. The thought behind this experiment was that citrate and DNA should both have their own selectivity profile towards different polyamine analogs, as confirmed from the ITC experiments done before. Upon modulating their capping ratio by adding more DNAs for displacing citrate, we expected to see a trend of change on the overall selectivity profile of AuNPs. However, not much difference among the tested conditions was observed after normalization. (Figure 6) It means DNA indeed had only weak or insignificant interactions with SPM and other polyamine analogs in causing any changes in the overall selectivity of AuNPs. Based on all of the evidences, we suspected citrate to be the key component in SPM-induced aggregation of AuNPs. This could also explain why Liu et al. reported a similar aggregation phenomenon of DNA-AuNPs using two DNAs with widely different base sequences, despite DNA-polyamine interaction was reported to be affected by factors like DNA conformation, base composition and sequence.[32,38] Another proof-of-concept experiment also indirectly indicated the importance of citrate groups: strong acid was added to DNA-AuNPs before adding SPM. It was found that SPM could not induce AuNPs

aggregation anymore in such an extreme acidic condition. We suspected it due to the complete protonation of citrate groups for further interaction with SPM, or even detachment from the surface of AuNPs.

Application of aptasensor in artificial and clinical urine

To demonstrate that the current developed aptasensor was fitted for its intended purpose for detecting SPM, its applicability was being tested in one of the most SPM-content concerning sample: urine. Artificial urine was prepared to mimic clinical urine during early investigation. Unfortunately, under the described optimal condition, the aptasensor failed to work properly since artificial urine is having a high salt concentration which could effectively screen negative charges for aggregation. AuNPs could not tolerate it even in the absence of SPM. The origin of such an undesired aggregation was a result of insufficient AuNPs protection by the surfactants. Clearly addition of only 25nM DNA was not enough for working in such complicated matrix and to provide further protection, the working DNA concentration was elevated to 250nM. Figure S13 showed the titration profile of DNA-AuNPs absorption spectrum against artificial urine with different dilution factor. With more matrix components, which were mainly inorganic salts, the absorbance of plasmonic peak declined gradually owing to the greater extent of DNA adsorption. Results showed that 250nM DNA was enough to protect AuNPs from aggregation up to two-fold diluted artificial urine.

SPM was spiked into artificial urine and Figure 7 showed the absorption spectrum and corresponding calibration curve. Surprisingly, AuNPs responded to SPM with a totally different mechanism compared to that in blank matrix. As revealed from the absorption pattern, with a higher SPM concentration, the plasmonic peak declined gradually similar to the previous titration study of artificial urine matrix effect. It confirmed that SPM could also help to screened negative charges like salts and induced further DNA adsorption.[39] Therefore a greater extent of DNA adsorption or even AuNPs precipitation were observed upon addition of SPM. (Figure S14) Both of them accounted for the drop of plasmonic band. The decrease was also found to correlate with SPM concentration with a linear relationship, and the LOD was calculated to be 473.29nM. A wider linear calibration curve from 0-18μM could be obtained which matched perfectly with that of general urinary SPM content. Spike analysis in artificial urine by a matrix-match calibration approach gave both satisfactory recovery and reproducibility.[40-41] (Table 2)

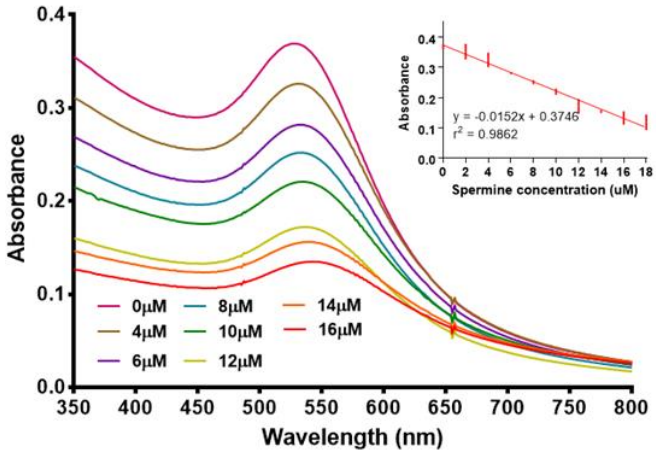

Figure 7. The SPM induced aggregation on DNA-AuNPs in artificial urine matrix - The absorption spectra of DNA-AuNPs upon addition of SPM solution. (0-18μM) Inset: Plot of Abs_{512} vs SPM concentration.

Table 2. Determination of spiked SPM in artificial urine specimen. (n=3)

Sample	Amount spiked (μM)	Average recovery (%)	Relative standard deviation (%)
Artificial urine	2.0	87.90	5.46
	4.0	100.61	0.07
	6.0	94.76	2.65
	8.0	106.70	2.01

To further demonstrate the applicability of the aptasensor for a fast urinary SPM screening, three clinical urine samples from cancerous patients were selected for further spike analysis. Before that, common urinary components (Urea, uric acid, glutathione, human serum albumin, calcium salt and creatinine) were tested to check if they interfered seriously with SPM sensing. (Figure S15) Results showed that only human serum albumin would cause slight AuNPs aggregation since protein is also a highly charged molecule. Therefore all the pre-spiked clinical urine samples were passed through Amicon centrifugal filter to remove any large protein molecules and then analyzed by the aptasensor again by a matrix-match calibration approach. The satisfactory accuracy and relative standard deviation values demonstrated the applicability of the aptasensor in real samples. (Table 3) More importantly, while in this work our design only focused on the detection of spermine, we believe the approach is modifiable and can be expanded for detecting other important DNA or even cancer-related miRNA by using a suitable complementary DNA sequence for adsorption.[42] This would find more potential applications in clinical diagnosis.

Table 3. Determination of spiked SPM in clinical urine specimen. (n=3)

Sample	Amount spiked (μM)	Average recovery (%)	Relative standard deviation (%)
Clinical urine 1	3.0	98.80	9.52
Clinical urine 2	3.0	121.98	7.76
Clinical urine 3	3.0	104.09	4.21

Conclusions

In conclusion, we have reported a smart and flexible aptasensor for SPM sensing simply by using the very common citrate-AuNPs and DNA aptamer for adsorption. Depending on the situation, users could tune the DNA concentration and the AuNPs would respond to SPM via two different mechanisms. When working in a comparatively clean matrix, a low DNA loading concentration was sufficient to protect AuNPs and simultaneously could provide a high sensitivity for SPM sensing. DNA-AuNPs will respond to it through the red-shifting of plasmonic band as the result of aggregation. When working in a complicated matrix like artificial urine, a high DNA loading concentration was needed to provide a better protection to AuNPs. The absorbance of plasmonic band would decrease gradually with a higher SPM concentration, which were accounted by a greater extent of DNA adsorption as well as precipitation of AuNPs. Different factors' effects were also comprehensively studied. Comparing to the target-mediated crosslinking mechanism, the use of non-thiolated DNA for preparing DNA-AuNPs was more easy, convenient and cost-effective. Good applicability in complicated urine matrices was also proven by the satisfactory results obtained in spike analysis. We foresee this novel approach to be a fast and practical kit towards SPM sensing and therefore prostate cancer screening.

Experimental Section

Materials and Instrument

All chemicals were acquired from Aldrich (Hong Kong, China) and Meryer (Shanghai, China). DNA aptamers (12mer: CGA CAA CCA CAA; 24mer: CGA CAA CCA CAA CAC ACA ATC TGA; 36mer: CGA CAA CCA CAA CAC ACA ATC TGA CGA CAA CCA CAA) were obtained from Invitrogen (Hong Kong, China). Britton-Robinson (BR) buffer was prepared by mixing equal molar ratio of phosphoric acid, boric acid and acetic acid. pH was then tuned using sodium hydroxide solution and a calibrated FiveEasy F20 Benchtop meter (Mettler-Toledo, Hong Kong, China). Artificial urine was prepared according to a recipe elsewhere with human serum albumin in place of chicken serum albumin.[43] All standard solutions were prepared in Milli-Q water. For urine samples, they were collected from suspected PCa patients from Princes of Wales Hospital, The Chinese University of Hong Kong under the approval of Clinical Research Ethical Committee. Details were described in a previously published literature.[21]

The transmission electron microscope (TEM) images of as-prepared AuNPs were captured using a JEOL Model JEM-2011

(JEOL, Beijing, China). Dynamic Light Scattering (DLS) and zeta-potential measurements were achieved by a Zetasizer Nano-ZS90 System (Malvern Instruments, Shanghai, China). The UV-Vis absorption spectra were recorded using a Cary 8453 UV-Vis Spectrometer (Agilent, Hong Kong, China). Isothermal Titration Calorimetry (ITC) study was achieved using MicroCal PEAQ-ITC Automated System (Malvern Instruments, Shanghai, China). All the incubations were performed on a KS 260 Basic Orbital Shaker (IKA, Hong Kong, China).

Synthesis of citrate-AuNPs

Three different sizes (4nm, 13nm, 27nm) of AuNPs were prepared. For 4nm citrate-AuNPs, the synthesis was performed according to a previous published literature by our group.[44] Briefly, chloroauric acid solution was mixed with trisodium citrate solution. Freshly-prepared sodium borohydride solution was then added and left for 2hr. For 13nm and 27nm AuNPs, the synthesis was done by the well-known Turkevich method, where trisodium citrate was used as both the reducing agent and capping ligands under refluxing condition.[45] Final sizes as determined from TEM were 4.09±0.65nm, 12.8±1.3nm and 27.2±4.2nm. (Figure 2) Concentration was calculated to be 114.54nM, 14.15nM and 1.53nM for 4, 13 and 27nm AuNPs respectively using equations suggested by Liu et al.[46] 4nm AuNPs were employed for majority of experiments, and different batches' absorbance and wavelength of plasmonic band did not show significant deviations.

Quantitative detection of spermine by AuNPs

Inside an Eppendorf tube, 80nM as-prepared 4nm AuNPs was vortex-mixed with 25nM DNA aptamer inside 4mM BR buffer (pH=3.29) for selective adsorption to take place. SPM standard/urine sample solution was then added and incubated for 60 min. The mixture was then ready for UV-Vis absorption, DLS and zeta-potential measurements. In complicated matrices like artificial urine and clinical urine, DNA concentration was raised to 250nM to provide a better protection.

Several parameters including AuNPs size (4, 13, 27nm), DNA aptamer concentration (12.5, 25, 50, 100 and 200nM), DNA length (12mer, 24mer and 36mer), pH (3.29, 4.96, 6.99, 8.98 and 11.0) and length of incubation time were studied and optimized based on the sensitivity towards SPM.

Urine sample pre-treatment

The clinical urine samples were thawed naturally and centrifuged for 5 min at 13000 rpm and room temperature. Then it was pre-treated with ultrafiltration (Amicon Ultra-15, MWCO = 3000Da) before use to remove any undesired interfering large molecules (e.g. proteins). For artificial urine, it was two-fold diluted before use without any further pre-treatments.

Isothermal titration calorimetry

For the study of interactions between DNA/citrate capped AuNPs and SPM, the AuNPs was again pre-concentrated using Amicon Ultra-15 3000Da centrifugal filter. Afterwards, 0.5μM AuNPs and different concentration of DNA aptamer (0, 0.5, 1 and 3μM) were mixed and placed into the sample cell. 0.25mM SPM solution was then gradually added for recording the temperature change per injection (2μL per injection in 150s interval at 25˚C).

For the study of interactions between citrate and polyamine analogues, 1mM trisodium citrate solution was placed into the sample cell. Different polyamine analogues solution was injected independently for recording the temperature under the above-mentioned conditions. Similarly, for the study of interactions between DNA and polyamine analogues, 10μM DNA solution was placed into the sample cell followed by addition of different polyamine solution.

In all cases the data were fitted by the single binding site model, integrated and analyzed by the MicroCal PEAQ-ITC Analysis software to obtain the dissociation constant, change of enthalpy, entropy and Gibbs free energy

Acknowledgements

The project was funded by University Research Facility for Chemical and Environmental Analysis (UCEA), and Area of Excellent Grants (1-ZVGG) of The Hong Kong Polytechnic University, Matching Proof-of-Concept Fund of Hong Kong Baptist University (MPCF-05-2016/17) and Shenzhen Science and Technology Innovation Committee (JCYJ20160330095659560 and JCYJ20150626111042525). The authors declare no competing financial interest.

Keywords: Spermine• Gold• Nanoparticles• DNA• Urine

[1] N. Seiler, J. G. Delcros, J. P. Moulinoux, *Int. J. Biochem. Cell Biol.* **1996**, *28*, 843-861.
[2] C. W. Tabor, H. Tabor, *Annu. Rev. Biochem.* **1976**, *45*, 285-306.
[3] B. G. Cipolla, J. Ziade, J. Y. Bansard, J. P. Moulinoux, F. Staerman, V. Quemener, B. Lobel, F. Guillé, *Cancer* **1996**, *78*, 1055-1065.
[4] C. Stefanelli, F. Bonavita, I. Stanic, M. Mignami, A. Facchinin, C. Pignatti, F. Flamigni, C. M. Calderera, *FEBS Lett.* **1998**, *437*, 233-236.
[5] E. W. Gerner, F. L. Meyskens, *Nat. Rev. Cancer* **2004**, *4*, 781-792.
[6] H. C. Ha, N. S. Sirisoma, P. Kuppusamy, J. L. Zweier, P. M. Woster, R. A. Casero, *Proc. Natl. Acad. Sci. USA* **1998**, *95*, 11140-11145.
[7] K. Igarashi, K. Kashiwagi, *Int. J. Biochem. Cell Biol.* **2010**, *42*, 39-51.
[8] H. T. Kurata, L. J. Marton, C. G. Nichols, *J. Gen. Physio.* **2006**, *127*, 467-480.
[9] A. N. Lopatin, E. N. Makhina, C. G. Nichols, *Nature* **1994**, *372*, 366-369.
[10] K. Williams, *Cell. Signal.* **1997**, *9*, 1-13.
[11] D. Russell, S. H. Snyder, *Proc. Natl. Acad. Sci. USA* **1968**, *60*, 1420-1427.
[12] D. H. Russell, C. C. Levy, S. C. Schimpff, I. A. Hawk, *Cancer Res.* **1971**, *31*, 1555-1558.
[13] S. H. Lee, Y. J. Yang, K. M. Kim, B. C. Chung, *Cancer Lett.* **2003**, *201*, 121-131.
[14] C. Löser, U. R. Fölsch, C. Paprotny, W. Creutzfeldt, *Cancer* **1990**, *65*, 958-966.
[15] J. Levêque, F. Foucher, J. Y. Bansard, R. Havouis, J. Y. Grall, J. P. Moulinoux, *Breast Cancer Res. Treat.* **2000**, *60*, 99-105.
[16] F. H. Schröder, A. B. Kruger, J. Rietbergen, R. Kranse, P. van der Maas, P. Beemsterboer, R. Hoedemaeker, *J. Natl. Cancer Inst.* **1998**, *90*, 1817-1823.
[17] M. Rigau, M. Olivan, M. Garcia, T. Sequeiros, M. Montes, E. Colás, M. Llauradó, J. Planas, I. Torres, J. Morote, C. Cooper, J. Reventós, J. Clark, A. Doll, *Int. J. Mol. Sci.* **2013**, *14*, 12620-12649.
[18] C. L. Wu, H. B. Carter, M. Naqibuddin, L. A. Fleisher, *Urology* **2001**, *57*, 925-929.
[19] E. S. Chan, K. L. Lo, C. F. Ng, S. M. Hou, S. K. Yip, *Chin. Med. J.* **2012**, *125*, 2432-2435.
[20] F. M. Wagenlehner, E. Van Oostrum, P. Tenke, Z. Tandogdu, M. Çek, M. Grabe, B. Wullt, R. Pickard, K. G. Naber, A. Pilatz, W. Weidner, T. E. Bjerklund-Johansen, *Eur. Urol.* **2013**, *63*, 521-527.
[21] T. H. Tsoi, C. F. Chan, W. L. Chan, K. F. Chiu, W. T. Wong, C. F. Ng, K. L. Wong, *PLoS One* **2016**, *11*, e0162217.
[22] N. N. Al-Hadithi, B. Saad, *Anal. Lett.* **2011**, *44*, 2245-2264.
[23] T. I. Kim, Y. Kim, *Chem. Commun.* **2016**, *52*, 10648-10651.
[24] S. Chopra, J. Singh, H. Kaur, A. Singh, N. Singh, N. Kaur, *Eur. J. Inorg. Chem.* **2015**, *2015*, 4437-4442.
[25] Y. J. Gu, J. Cheng, C. W. Y. Man, W. T. Wong, S. H. Cheng, *Nanomedicine: NBM* **2012**, *8*, 204-211.
[26] G. Sener, L. Uzun, A. Denizli, *Anal. Chem.* **2013**, 86(1), 514-520.
[27] Y. Guo, Y. Zhang, H. Shao, Z. Wang, X. Wang, X. Jiang, *Anal. Chem.* **2014**, *86*, 8530-8534.
[28] J. J. Feng, H. Guo, Y. F. Li Y. H., Wang, W. Y. Chen, A. J. Wang, *ACS Appl. Mater. Inter.* **2013**, *5*, 1226-1231.
[29] N. Jornet-Martinez, M. González-Béjar, Y. Moliner-Martínez, P. Campins-Falco, J. Pérez-Prieto, *Anal. Chem.* **2014**, *86*, 1347-1351.
[30] T. I. Kim, J. Park, Y. Kim, *Chem. - Eur. J.* **2011**, *17*, 11978-11982.
[31] K. A. Rawat, J. R. Bhamore, R. K. Singhal, S. K. Kailasa, *Biosens. Bioelectron.* **2017**, *88*, 71-77.
[32] Z. D. Liu, H. Y. Zhu, H. X. Zhao, C. Z. Huang, *Talanta* **2013**, *106*, 255-260.
[33] X. Zhang, M. R. Servos, J. Liu, *Langmuir* **2012**, *28*, 3896-3902.
[34] A. H. Malik, S. Hussain, P. K. Iyer, *Anal. Chem.* **2016**, *88*, 7358-7364.
[35] D. Rautaray, S. Mandal, M. Sastry, *Langmuir* **2005**, *21*, 5185-5191.
[36] J. E. Morgan, J. W. Blankenship, H. R. Matthews, *Arch. Biochem. Biophys.* **1986**, *246*, 225-232.
[37] J. W. Park, J. S. Shumaker-Parry, *J. Am. Chem. Soc.* **2014**, *136*, 1907-1921.
[38] Z. Bagheryan, A. Noori, S. Z. Bathaie, M. Yousef-Elahi, M. F. Mousavi, Biosens. Bioelectron. **2016**, *77*, 767-773.

[39] K. Gracie, M. Moores, W. E. Smith, K. Harding, M. Girolami, D. Graham, K. Faulds, *Anal. Chem.* **2016**, *88*, 1147-1153.
[40] A. Xiong, Y. Li, L. Yang, J. Gao, Y. He, C. Wang, Z. J. Wang, *Pharm. Biomed. Anal.* **2009**, *50*, 1070-1074.
[41] T. H. Tsoi, W. T. Wong, *Anal. Methods* **2015**, *7*, 5989-5995.
[42] X. Zhou, P. Cao, Y. Zhu, W. Lu, N. Gu, C. Mao, *Nat. Mater.* **201**5, *14*, 1058-1064.
[43] A. Álvarez, J. M. Costa, R. Pereiro, A. Sanz-Medel, *Sens. Actuators, B* **2012**, *168*, 370-375.
[44] Y. J. Gu, J. Cheng, C. C. Lin, Y. W. Lam, S. H. Cheng, W. T. Wong, Toxicol. *Appl. Pharm.* **2009**, *237*, 196-204.
[45] J. Turkevich, P. C. Stevenson, J. Hillier, *Discuss. Faraday Soc.* **1951**, *11*, 55-75.
[46] X. Liu, M. Atwater, J. Wang, Q. Huo, *Colloids Surf., B* **2007**, *58*, 3-7.

Supporting Information

Table of content

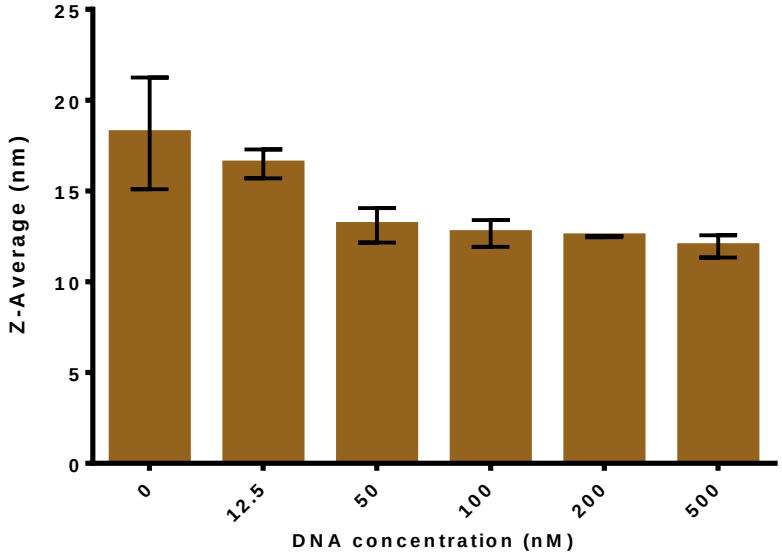

Figure S1. DNA adsorption effect on DLS results of AuNPs. (AuNPs: 80nM in 4mM BR-buffer, pH=3.29)

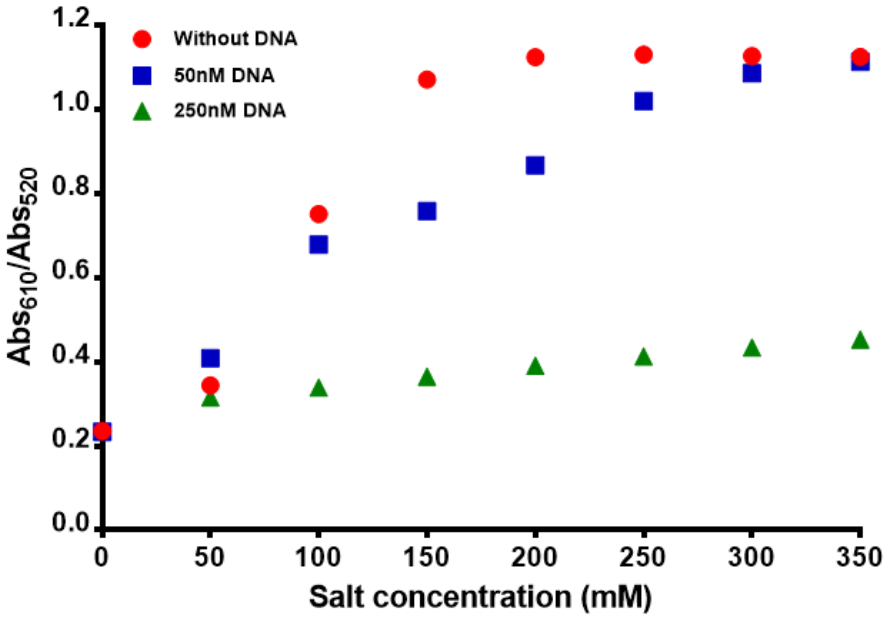

Figure S2. DNA protection effect against 4nm AuNPs aggregation at different NaCl concentration. (0, 50 and 250nM)

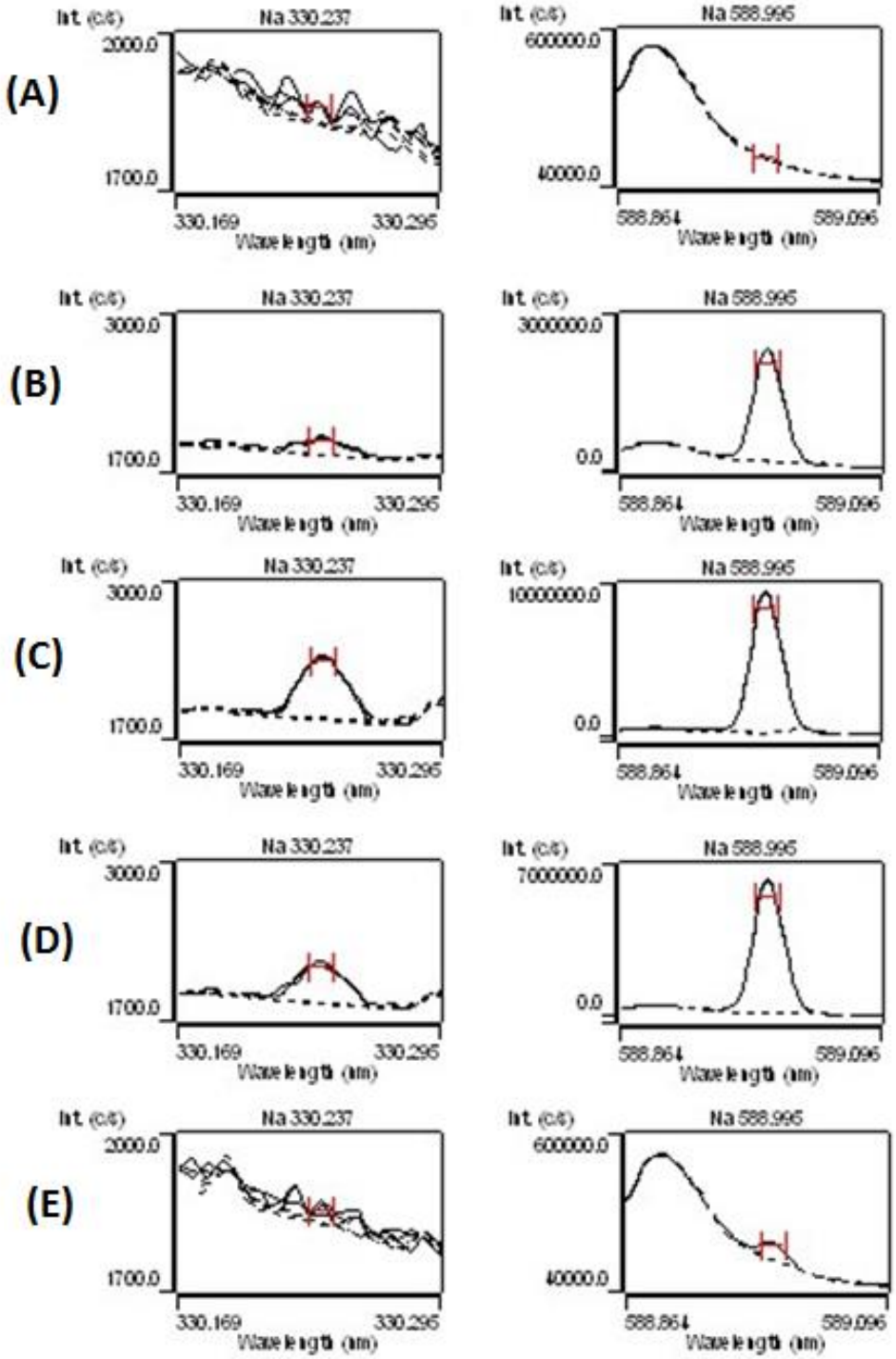

Figure S3. Emission peak of Na at 330.237nm and 588.995nm measured by ICP-OES. (A) 1% HNO_3 (Blank) (B) 2ppm Na (C) 10ppm Na (D) Stock AuNPs (E) Ultra-filtration-treated AuNPs

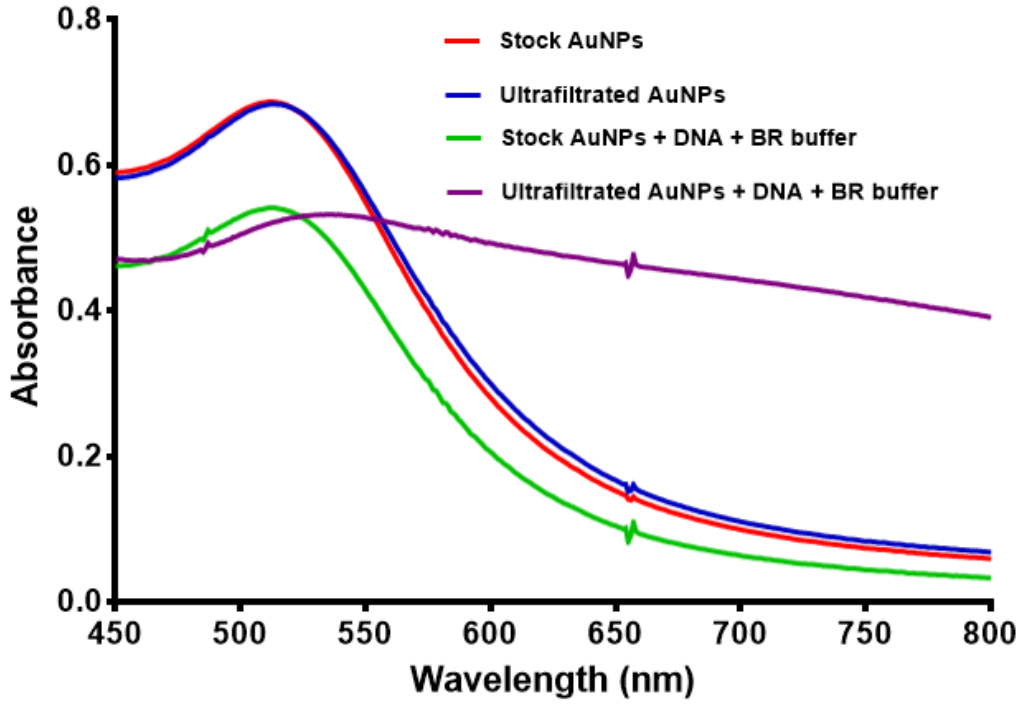

Figure S4. Absorption spectra of (A) Stock AuNPs (B) Ultra-filtrated AuNPs (C) Stock AuNPs in the presence of DNA and BR buffer, pH 3.29 (D) Ultra-filtrated AuNPs in the presence of DNA and BR buffer, pH 3.29.

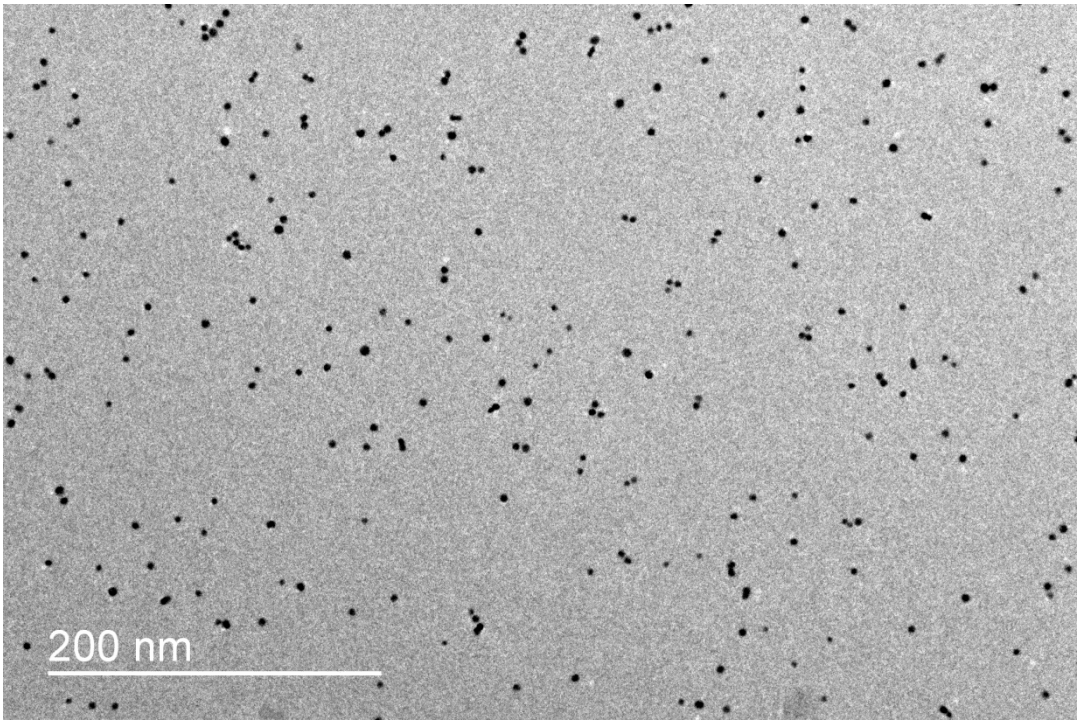

Figure S5. TEM image of AuNPs after ultrafiltration.

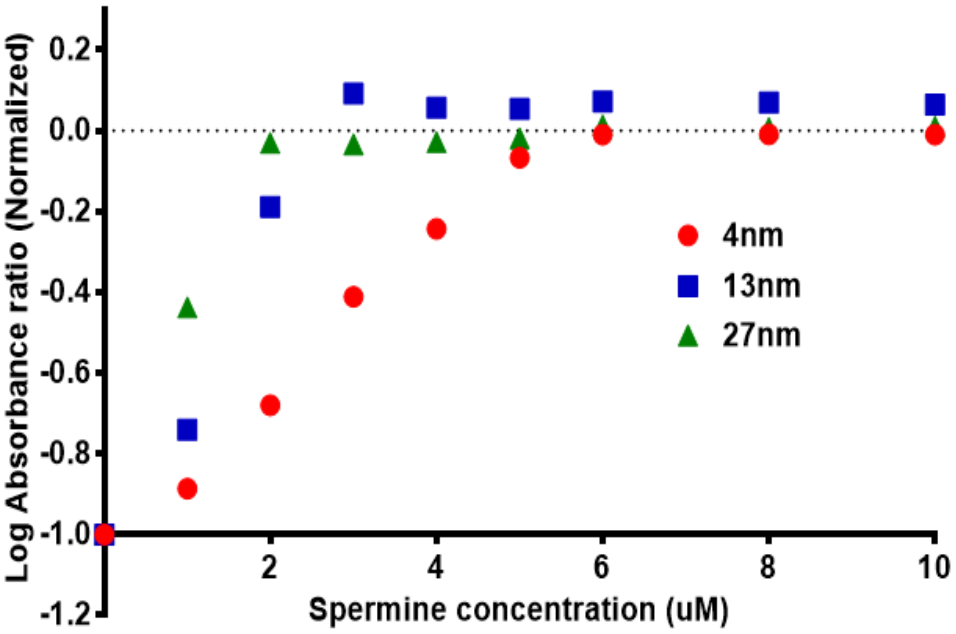

Figure S6. AuNPs size effect on calibration graph of spermine. (DNA concentration: 25nM; pH=3.29; AuNPs concentration: 80nM for 4nm, 2.38nM for 13nm, 0.24nM for 27nm; concentration was chosen such that they gave similar absorbance value at their plasmonic peak; Plasmonic peak wavelength: 512nm for 4nm, 523nm for 13nm, 532nm for 27nm)

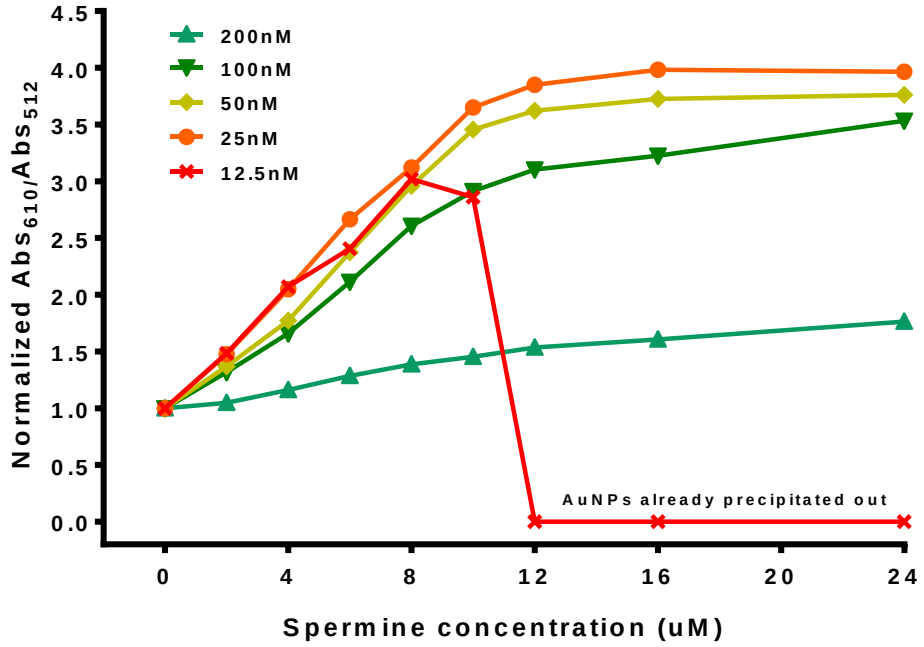

Figure S7. DNA concentration effect on spermine calibration graph. (4nm AuNPs: 80nM, pH: 3.29)

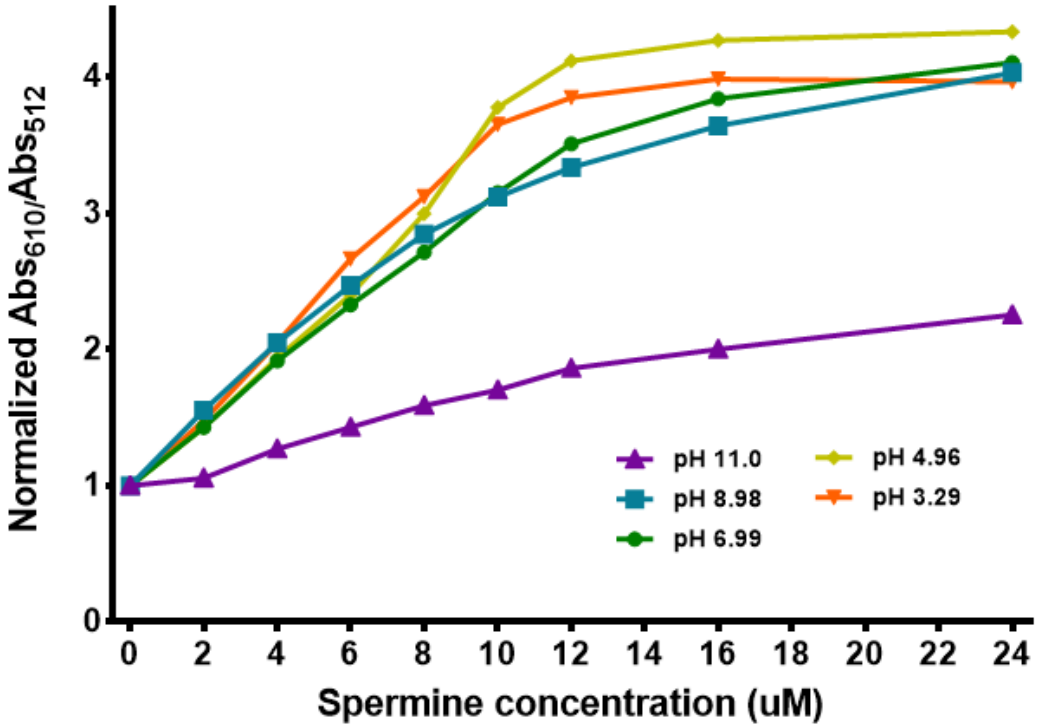

Figure S8. pH effect on spermine calibration graph. (4nm AuNPs: 80nM, DNA: 25nM)

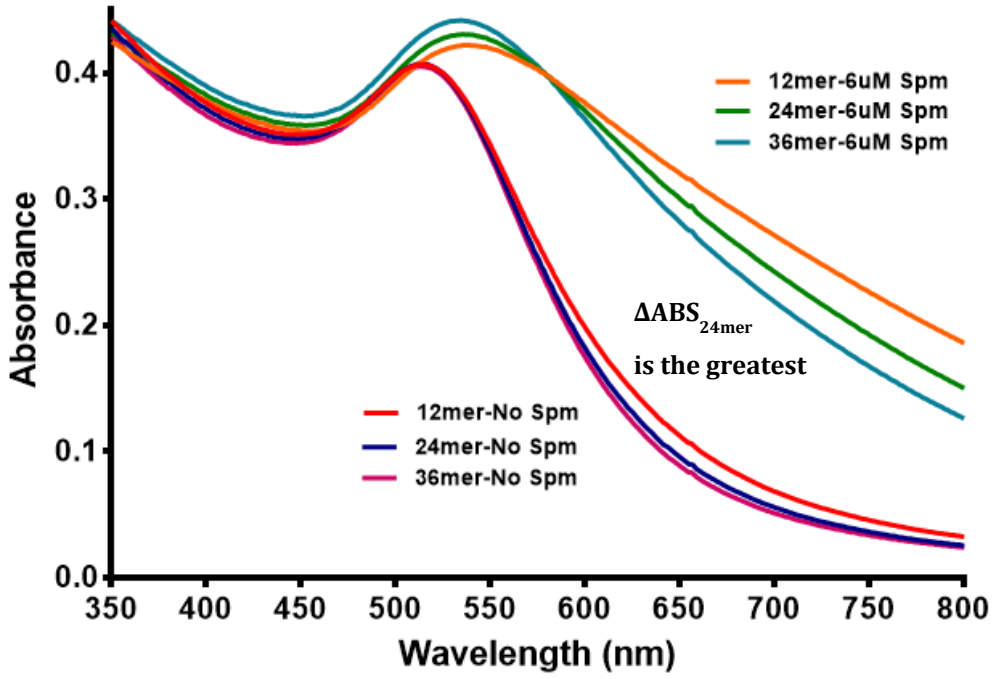

Figure S9. Absorption spectra of AuNPs capping with DNA of different length (DNA sequence: 12mer: CGA CAA CCA CAA; 24mer: CGA CAA CCA CAA CAC ACA ATC TGA; 36mer: CGA CAA CCA CAA CAC ACA ATC TGA CGA CAA CCA CAA)

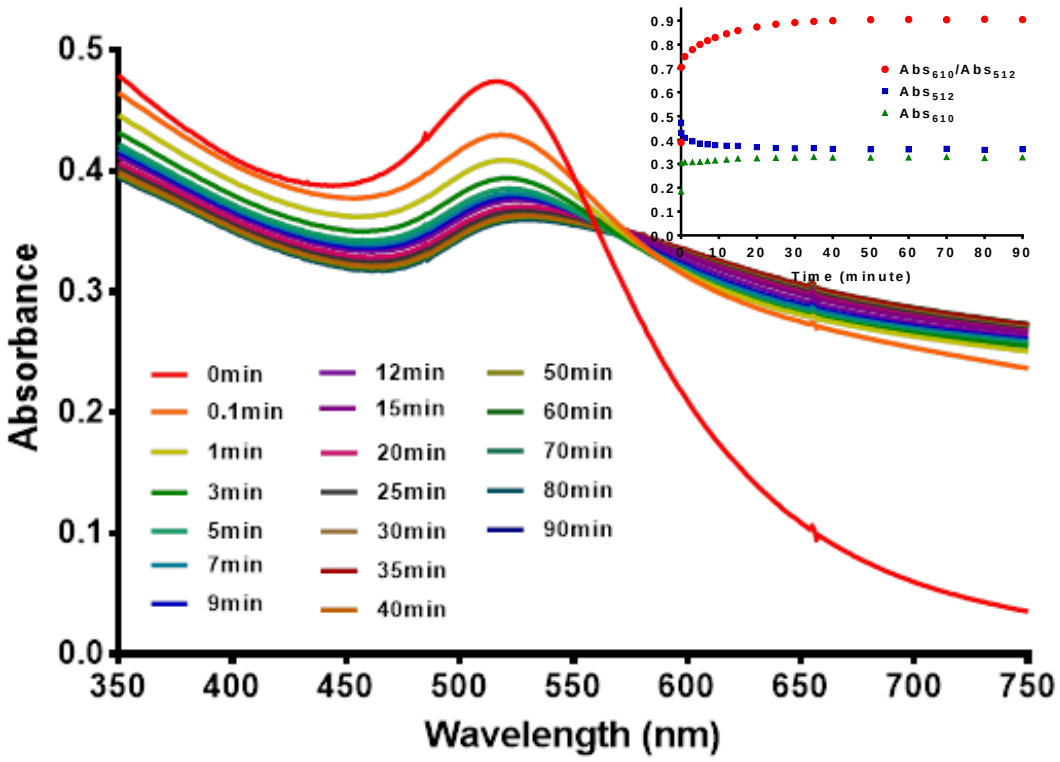

Figure S10. Kinetics for spermine-induced aggregation of DNA-AuNPs. (AuNPs: 80nM; DNA: 25nM; Spermine: 6μM) Inset: Abs_{610}, Abs_{512} & their ratio against time.

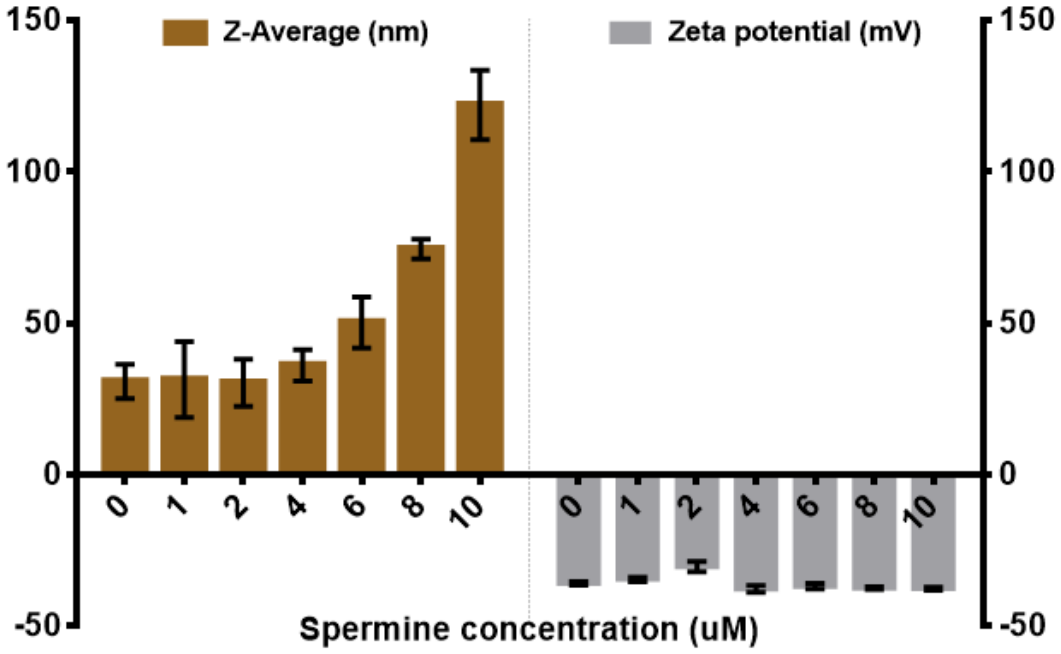

Figure S11. DLS and zeta-potential measurements of DNA capped AuNPs with different extent of spermine-induced aggregation.

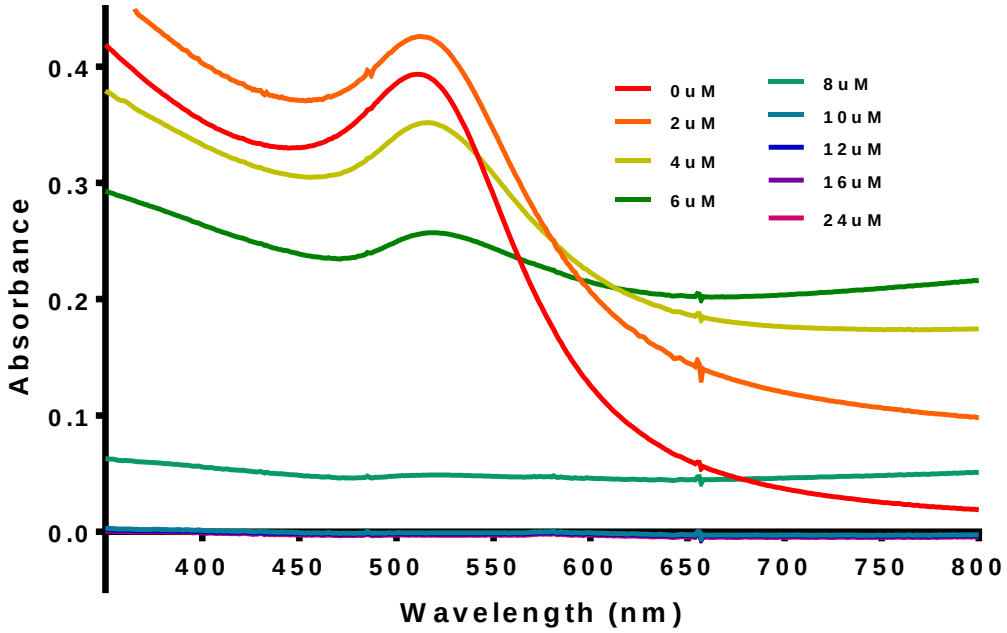

Figure S12. Absorption spectra of AuNPs upon addition of spermine solution (0-24μM) in the absence of DNA.

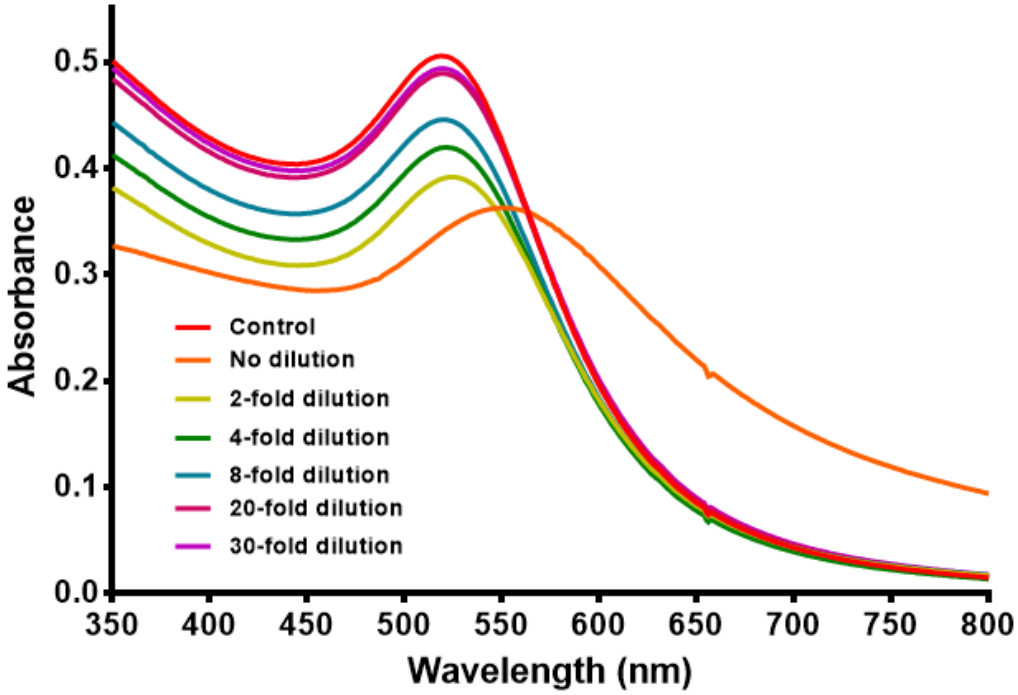

Figure S13. Absorption spectra of DNA-AuNPs upon addition of artificial urine with different dilution factor.

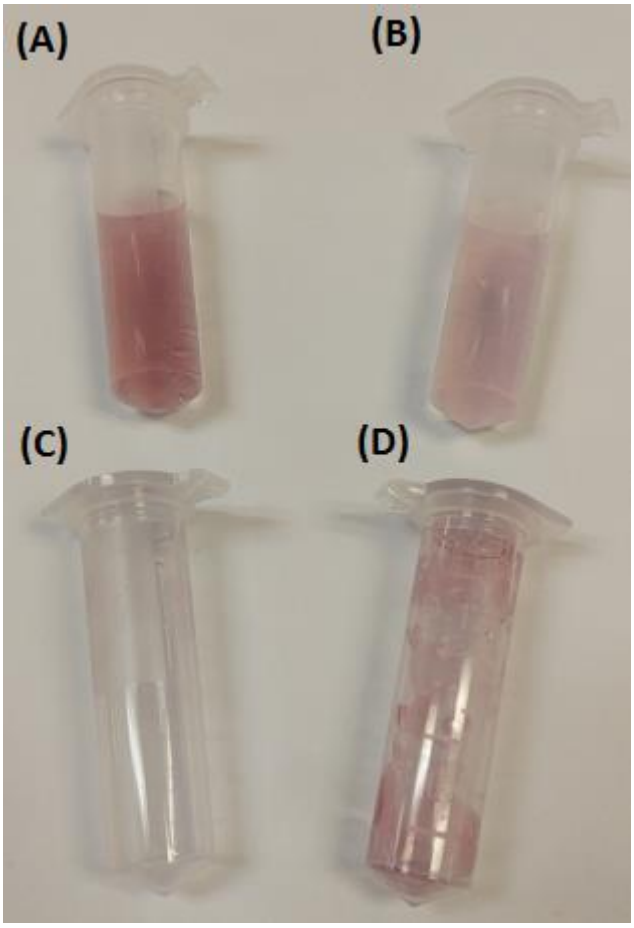

Figure S14. Color of AuNPs solution after incubating with (A) 0μM and (B) 16μM Spm (Concentration: AuNPs = 80nM; DNA concentration =250nM; BR buffer, pH3.29) Appearance of remaining reaction Eppendorf tube after incubation with (C) 0μM and (D) 16μM Spm.

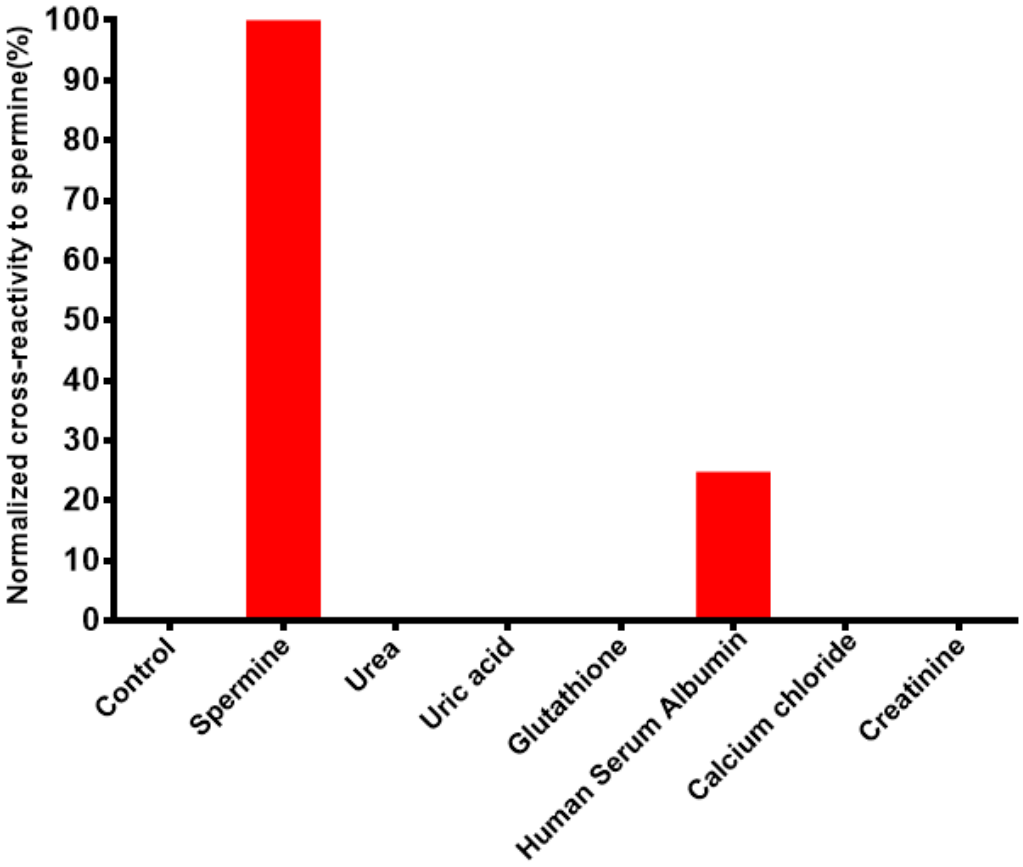

Figure S15. Cross-reactivity of urinary components to spermine by developed aptasensor. In each case control (water) and spermine were normalized to 0 and 100% respectively. (Concentration used = 4µM)

DNA concentration (nM)	Equation	R^2	Linear range
12.5	y = 0.2305x + 1.0134	0.9975	0-4uM
25	y = 0.2657x + 0.9893	0.9988	0-6uM
50	y= 0.2258x + 0.9987	0.9968	0-10uM
100	y = 0.1972x + 1.0578	0.9959	0-10uM
200	y = 0.0529x + 0.9981	0.9926	0-16uM

Table S1. Summarized results on the linear equation, R^2 and linear range of spermine calibration graphs at different DNA concentration.

pH	Equation	R^2	Linear range
3.29	y = 0.2657x + 0.9893	0.9988	0-6µM
4.96	y= 0.2510x + 0.9708	0.9944	0-10µM
6.99	y = 0.2021x + 1.0845	0.9945	0-12µM
8.98	y = 0.2321x + 1.0862	0.9914	0-8µM
11.0	y = 0.0822x + 0.8323	0.9996	2-8µM

Table S2. Summarized results on the linear equation, R^2 and linear range of spermine calibration graphs at different pH.

Analytes	Fitness of binding model	K_D (M)	ΔH (kcal/ mol)	ΔG (kcal/ mol)	TΔS (kcal/ mol)
Spermine	Good	1.26 x10^{-6}	-36.9	-8.05	-28.8
Spermidine	Good	2.11 x10^{-6}	-18.4	-7.74	-10.7
Histamine	Moderate	6.56 x10^{-3}	-15.6	-2.98	-12.7
Putrescine	Good	1.41 x10^{-6}	-14.5	-7.98	-6.54
Arginine	Poor	3.65 x10^{-3}	-6.45	-3.33	-3.13
Tyramine	Poor	3.88 x10^{-6}	-0.24	-7.38	7.14
Cadaverine	Cannot be fitted	N/A	N/A	N/A	N/A
Ornithine	Cannot be fitted	N/A	N/A	N/A	N/A
Control (water)	Cannot be fitted	N/A	N/A	N/A	N/A

Table S3. Thermodynamic parameters of the binding of citrate to different polyamine analogs.

Analyte	Fitness of binding model	K_D (M)	ΔH (kcal/ mol)	ΔG (kcal/ mol)	TΔS (kcal/ mol)
Spermine	Good	1.10 x10^{-6}	-7.83	-8.13	0.308
Spermidine	Good	1.11 x10^{-6}	-4.44	-8.13	3.69
Histamine	Good	1.27 x10^{-5}	-3.61	-6.68	3.07
Putrescine	Good	3.97 x10^{-6}	-7.29	-7.37	0.08
Arginine	Good	1.42 x10^{-5}	-4.59	-6.61	2.03
Tyramine	Good	3.06 x10^{-5}	-13.6	-6.16	-7.46
Cadaverine*	Good	9.33 x 10^{-6}	1.06	-6.86	7.93
Ornithine	Cannot be fitted	N/A	N/A	N/A	N/A
Control (water)	Cannot be fitted	N/A	N/A	N/A	N/A

** Cadaverine interacted with DNA following an endothermic pathway.*

Table S4. Thermodynamic parameters of the binding of DNA to different polyamine analogs.